J|A|C|S ARTICLES

Published on Web 12/10/2009

Anisotropic Etching of Silver Nanoparticles for Plasmonic Structures Capable of Single-Particle SERS

Martin J. Mulvihill, Xing Yi Ling, Joel Henzie, and Peidong Yang*

Department of Chemistry, University of California, Berkeley, California 94720, and Materials Sciences Division, Lawrence Berkeley National Laboratory, Berkeley, California 94720

Received August 16, 2009; E-mail: p_yang@berkeley.edu

Abstract: The understanding of the localized surface plasmons (LSPs) that occur at the geometrically bounded surface of metal nanoparticles continues to advance as new and more complex nanostructures are found. It has been shown that the oscillation of electrons at the metal dielectric interface is strongly dependent on the size, symmetry, and proximity of nanoparticles. Here, we present a new method to chemically control the shape of silver nanocrystals by using a highly anisotropic etching process. Tuning of the etchant strength and reaction conditions allows the preparation of new nanoparticle shapes in high yield and purity, which cannot be synthesized with conventional nanocrystal growth methods. The etching process produces intraparticle gaps, which introduce modified plasmonic characteristics and significant scattering intensity in the near-infrared. These new silver particles serve as excellent substrates for wavelength-tunable, single-particle surface enhanced Raman spectroscopy (spSERS).

Introduction

The emergence of plasmonics in nanoscale materials has led to increased interest in the fundamental understanding of localized surface plasmons in metal nanostructures, particularly those with well-defined shapes and sizes.[1−6] The synthesis of well-defined metal nanoparticles with distinct plasmon scattering signatures has led to the development of new techniques including surface enhanced Raman scattering (SERS)[7] and surface plasmon resonance (SPR).[8] Metal nanoparticles have also been used in a variety of applications including light emitting diodes,[9] sensors,[10,11] biological imaging,[12] single molecule spectroscopy,[13] and cancer therapies.[14,15] The creation and examination of numerous metal nanoparticle shapes, sizes, and assemblies has demonstrated the importance of each of these parameters to tailor the resulting plasmonic characteristics of these materials.[1,3,4,16−18] For example, by changing the shape of silver nanoparticles from cubes to cube-octahedra to octahedra, we can create increasingly sensitive SERS substrates.[11] These particles, which can be as large as 300 nm in diameter, have broad dipolar resonances and show many of the higher-order modes not seen in other smaller particles. The broad-band nature of large particles scattering profiles along with the ability to finely control particle morphology makes these shapes ideal starting materials for further investigation. By controlling the shape of these silver particles, we will show that the localized surface plasmons (LSPs) can be shifted into the near-infrared through an intraparticle rather than the more common interparticle coupling mechanism.[19,20]

In this report, we demonstrate the ability to chemically modify the optical properties of plasmonic nanoparticles by changing their morphology using an anisotropic etching technique. These etched particles possess unique structural features that exhibit single-particle SERS (spSERS) signals 30 times stronger than the original structures, making them very appealing as Raman

(1) Jackson, J. B.; Halas, N. J. *Proc. Natl. Acad. Sci. U.S.A.* **2004**, *101*, 17930–17935.
(2) Wiley, B.; Sun, Y. G.; Xia, Y. *Acc. Chem. Res.* **2007**, *40*, 1067–1076.
(3) Nehl, C. L.; Liao, H. W.; Hafner, J. H. *Nano Lett.* **2006**, *6*, 683–688.
(4) Tao, A.; Sinsermsuksakul, P.; Yang, P. D. *Angew. Chem. Int. Ed.* **2006**, *45*, 4597–4601.
(5) Wang, H.; Brandl, D. W.; Nordlander, P.; Halas, N. J. *Acc. Chem. Res.* **2007**, *40*, 53–62.
(6) Rodriguez-Lorenzo, L.; Alvarez-Puebla, R. A.; Pastoriza-Santos, I.; Mazzucco, S.; Stephan, O.; Kociak, M.; Liz-Marzan, L. M.; de Abajo, F. J. G. *J. Am. Chem. Soc.* **2009**, *131*, 4616–4618.
(7) Haynes, C. L.; McFarland, A. D.; Van Duyne, R. *Anal. Chem.* **2005**, *77*, 338A–346A.
(8) Zhao, J.; Das, A.; Zhang, X. Y.; Schatz, G. C.; Sligar, S. G.; Van Duyne, R. P. *J. Am. Chem. Soc.* **2006**, *128*, 11004–11005.
(9) Okamoto, K.; Niki, I.; Shvartser, A.; Narukawa, Y.; Mukai, T.; Scherer, A. *Nat. Mater.* **2004**, *3*, 601–605.
(10) Stuart, D. A.; Yuen, J. M.; Lyandres, N. S. O.; Yonzon, C. R.; Glucksberg, M. R.; Walsh, J. T.; Van Duyne, R. P. *Anal. Chem.* **2006**, *78*, 7211–7215.
(11) Mulvihill, M.; Tao, A.; Benjauthrit, K.; Arnold, J.; Yang, P. *Angew. Chem. Int. Ed.* **2008**, *47*, 6456–6460.
(12) Hirsch, L. R.; Gobin, A. M.; Lowery, A. R.; Tam, F.; Drezek, R. A.; Halas, N. J.; West, J. L. *Ann. Biomed. Eng.* **2006**, *34*, 15–22.
(13) Dieringer, J. A.; Lettan, R. B.; Scheidt, K. A.; Van Duyne, R. P. *J. Am. Chem. Soc.* **2007**, *129*, 16249–16256.
(14) Chen, J. Y.; Wang, D. L.; Xi, J. F.; Au, L.; Siekkinen, A.; Warsen, A.; Li, Z. Y.; Zhang, H.; Xia, Y. N.; Li, X. D. *Nano Lett.* **2007**, *7*, 1318–1322.
(15) Gobin, A. M.; Lee, M. H.; Halas, N. J.; James, W. D.; Drezek, R. A.; West, J. L. *Nano Lett.* **2007**, *7*, 1929–1934.
(16) Jin, R. C.; Cao, Y. W.; Mirkin, C. A.; Kelly, K. L.; Schatz, G. C.; Zheng, J. G. *Science* **2001**, *294*, 1901–1903.
(17) Tao, A.; Sinsermsuksakul, P.; Yang, P. D. *Nat. Nanotechnol.* **2007**, *2*, 435–440.
(18) Orendorff, C. J.; Gole, A.; Sau, T. K.; Murphy, C. J. *Anal. Chem.* **2005**, *77*, 3261–3266.
(19) Driskell, J. D.; Shanmukh, S.; Liu, Y.; Chaney, S. B.; Tang, X. J.; Zhao, Y. P.; Dluhy, R. A. *J. Phys. Chem. C* **2008**, *112*, 895–901.
(20) Talley, C. E.; Jackson, J. B.; Oubre, C.; Grady, N. K.; Hollars, C. W.; Lane, S. M.; Huser, T. R.; Nordlander, P.; Halas, N. J. *Nano Lett.* **2005**, *5*, 1569–1574.

10.1021/ja906954f

sensors.[6,11,13,21−25] Importantly, these structures demonstrate that interparticle gaps are not always essential for a strong SERS response. These single-crystalline particles are produced in large quantities and have uniform spSERS responses between particles. As the shapes of the particles are changed through anisotropic etching, the various shapes demonstrate a wavelength-dependent SERS response that corresponds to the changes seen in the particle scattering features. This allows single silver particles to act as reproducible spSERS substrates with excitation wavelengths as long as 785 nm.

Unlike previous reports[21−23] of spSERS, our nanoparticles are sensitive enough to detect nonresonant analytes. In addition, because these earlier reports also rely on the gaps and junctions of randomly assembled small particle aggregates ranging in size from 100−300 nm, only 1% of such structures were spSERS-active substrates.[13,21] Recent work from the Xia's group has shown that single silver nanoparticles are attractive candidates for nonresonant, spSERS applications.[24,25] Our synthetic strategy improves on these results by generating large quantities of anisotropically shaped particles at similar size scales with precisely tunable intraparticle gaps that affect their spSERS response. The results of our shape-dependent spSERS experiments demonstrate that key features for SERS enhancement, including both sharp corners and gaps, can be incorporated into a single-crystalline, single-particle sensing platform.

The development of chemical methods that have the ability to simultaneously control particle shape, size, and composition on the nanoscale has been fundamental to the emergence of nanotechnology.[2,26,27] A key strategy for controlling the shape of single-crystalline nanoparticles is the ability to distinguish between various crystallographic faces and growth directions. In this report, we show that a simple chemical etchant can be used to generate complex particle architectures by examining the opposite of the nanocrystal *growth*, that is selective *etching* of shaped nanoparticles. Our anisotropic etching technique exploits many of the same chemical concepts used to control the shape of nanostructures during the growth process, and by considering the relationship between these seemingly opposite transformations; insight is gained into the mechanisms of both.[24] Reaction parameters including solvent, temperature, and time have all been shown to influence the particle morphology during the growth process. These same parameters could influence the resulting particle morphology during the etching process. In this regard, we have developed a simple etchant system for silver nanoparticles that selectively etches the (100) planes of the nanocrystals. By using poly(vinylpyrrolidone) (PVP) as a stabilizing agent for these metallic particles, we are able to isolate complex particle shapes that are resistant to oxidation and can readily be modified with other surface functionalities.[11]

Experimental Section

General. Hydrogen peroxide (30%) in water and concentrated ammonium hydroxide were purchased from Fisher Scientific. 1,5-pentanediol (98%) was purchased from Acros Organics. All other chemicals were purchased from Sigma Aldrich. Nanopure (>18.0 MΩ) water was purified with a Barnstead B-Pure system. UV−vis−NIR spectra were measured using a Shimadzu UV-3101 PC spectrophotometer. Scanning electron micrographs were obtained using a field emission scanning electron microscope (FESEM, JEOL6430). Images were obtained with an operating voltage of 5 kV.

Nanoparticle Synthesis. This synthesis, which was first reported by our lab in 2006,[4] has undergone minor changes that allow for the easier isolation of polyhedral silver nanocrystals. Silver nitrate (0.20 g) and copper(II) chloride (0.86 mg) were dissolved in 1,5-pentanediol (10 mL) in a glass vial. In a separate vial, PVP (M_w = 55 000 amu, 0.10 g) was dissolved in 1,5-pentanediol (10 mL). All solutions were dissolved using ultrasonic baths. The resulting silver nitrate solution is a slightly opaque yellow-orange solution, and usually takes about 30 min to completely dissolve.

Using a temperature-controlled silicone oil bath, 1,5-pentanediol (20 mL) was heated for 10 min in the 190 °C oil bath. The purity and heating time of the 1,5-pentanediol can greatly influence the yield of the reactions. The two precursor solutions were then injected into the hot reaction flask at the following rates: 500 μL of the silver nitrate solution every minute and 250 μL of the PVP solution every 30 s. For nanocubes, this addition was stopped once the solution turned opaque (∼14 min). The reaction can be paused at this point to evaluate the cube product using UV−vis and SEM before proceeding with the reaction to make cubeoctahedra or octahedra. To resume the reaction, the mixture was heated for 10 min at 190 °C for 10 min and then the injections of silver nitrate and PVP solutions were resumed. For cuboctahedra and octahedra, the addition of precursor solutions was continued for a longer period of time: 30−45 min for cube-octahedra and 60−75 min for octahedra nanocrystals.

Nanoparticle Etching. Unless otherwise noted, etching experiments were all carried out at 4 °C and with an etchant solution of 9 parts concentrated ammonium hydroxide and 1 part 30% hydrogen peroxide. This solution was always freshly prepared and kept on ice. To a solution of PVP and DI water (1 mg/mL) an aliquot of etchant was added while vigorously stirring and then an aliquot of silver nanoparticles was rapidly injected. The solution immediately changed color and evolved gas; the reaction ran to completion in a matter of seconds and was allowed to stir for 5 min. In a typical reaction, 4.5 mL of the PVP water solution, 200 μL of etchant, and 500 μL of silver particles in ethanol were used. The etched particles were then isolated by centrifugation (12 000 rpm, 3 min) and then washed numerous times with water and stored in ethanol.

Darkfield Scattering Measurements. All scattering measurements were performed on a darkfield inverted microscope (Olympus IX71). Dilute colloidal solutions of nanocrystals were drop-cast onto a clean glass coverslip and measured in air. The samples were illuminated with a 100 W halogen bulb using a darkfield condenser (NA = 0.8−0.92). Darkfield images and spectra were obtained from scattered light collected through a 60× microscope objective lens (NA = 0.7) and coupled to a 0.3 m spectrometer (PI-Acton, SpectraPro 2300i) equipped with a 1340 × 400 pixel back-illuminated CCD camera (PI-Acton, Spec-10:400B). To obtain corrected single-particle scattering spectra the background from the glass slide was subtracted and then divided by the lamp spectra.

Raman Spectroscopy. Samples were prepared by drop casting a dilute solution of particles suspending in ethanol onto a silicon wafer with evaporated chromium pads, which were used as markers for SEM correlation. Benzenethiol-coated samples were prepared for Raman spectroscopy by first exchanging the PVP with BT in a

(21) Doering, W. E.; Nie, S. M. *J. Phys. Chem. B* **2002**, *106*, 311–317.
(22) Camden, J. P.; Dieringer, J. A.; Wang, Y. M.; Masiello, D. J.; Marks, L. D.; Schatz, G. C.; Van Duyne, R. P. *J. Am. Chem. Soc.* **2008**, *130*, 12616–12617.
(23) Michaels, A. M.; Nirmal, M.; Brus, L. E. *J. Am. Chem. Soc.* **1999**, *121*, 9932–9939.
(24) Cobley, C. M.; Rycenga, M.; Zhou, F.; Li, Z. Y.; Xia, Y. N. *Angew. Chem. Int. Ed.* **2009**, *48*, 4824–4827.
(25) McLellan, J. M.; Siekkinen, A.; Chen, J. Y.; Xia, Y. N. *Chem. Phys. Lett.* **2006**, *427*, 122–126.
(26) Peng, X. G.; Manna, L.; Yang, W. D.; Wickham, J.; Scher, E.; Kadavanich, A.; Alivisatos, A. P. *Nature* **2000**, *404*, 59–61.
(27) Sun, Y. G.; Xia, Y. N. *Science* **2002**, *298*, 2176–2179.

20 mM ethanolic solution, which was stirred for 12 h at room temperature under a stream of N_2 to minimize oxidation. The samples were then thoroughly rinsed and dried under nitrogen before transferring to the microscope stage for immediate spectral collection. All mapping experiments were carried out with a 100× objective lens (NA = 0.85) and were taken using 1 s accumulations between 1350 and 1850 cm^{-1}. The lasers used include a 514 nm argon ion laser, a 633 nm diode laser, and a 785 diode laser. To obtain single-particle spectra, laser powers of 0.7, 1.2, 1.2 mW were used for 514, 633, and 785 nm excitations, respectively. A 100× objective lens with a NA = 0.85 was used to focus and collect the light. Automated mapping software was used to control the movement of the stage in 0.5 μm steps during the mapping experiments. Use of the confocal pinhole ensured that the illumination area for each of the wavelengths was comparable. After the Raman mapping was complete, the chromium pads aided in pattern matching with SEM images to ensure that only single particles were used for quantification. Enhancement factors for these particles were estimated using the expression $EF = (I_{surface})/(I_{solution}) \times N_{solution}/N_{surface}$. Intensities for the EF were taken for both single particles and neat BT using identical laser power. $N_{solution}$ was calculated from the probe volume of a BT solution in a 100 μm thick glass cell solution assuming a diffraction limited spot with a 20× objective (NA = 0.4). $N_{surface}$ was determined by a geometric estimation of the particle surface area and the van der Waals dimensions of the thiol headgroup (2.3 × 2.3 $Å^2$), assuming a close-packed monolayer of BT.

Results and Discussion

Transforming PVP-coated silver nanocrystals into different shapes is enabled in part by the low reduction potential of silver (Supporting Information for associated reaction potentials). Methods such as galvanic displacement[28−30] and redox mediated etching[24] have produced alloy and cage structures from noble metal nanocrystal starting materials. The particles formed here using a crystallographically selective etchant give access to a new class of nanomaterials with tunable intraparticle gaps. During etching reactions on nanoscale materials, the strength of the etchant must be carefully chosen: an etchant that is too strong will etch the nanoparticle isotropically, whereas an etchant that is too weak may not be able to react with the particle surface in the presence of capping agents. The appropriate etchants for nanoscale gold have been reported[31,32] and for bulk silver a mixture of ammonium hydroxide, hydrogen peroxide, and chromic acid has been shown to selectively etch pits in dislocations on silver (100) and (111) surfaces.[33] The etchant for bulk silver consists of 5 parts concentrated NH_4OH, 1 part 30% H_2O_2, and 0.08 parts by volume of a solution consisting of 5 g CrO_3, 25 mL DI water, and 0.5 mL concentrated HCl. We hypothesized that an etchant selective for high-energy surfaces would be able to introduce anisotropy into our single-crystalline silver nanocrystals by preferentially reacting at edges and corners.

To apply this etchant formulation to a nanoparticle solution, much smaller concentrations must be used. Instead of using neat etchant solutions, a small amount of the etchant formulation was added to a solution of PVP in water. This diluted solution typically contained less than 500 μL of the etchant in 4.5 mL of a 1 mg/mL solution of PVP/H_2O. By making the etchant the limiting reagent in a solution of our octahedral silver nanoparticles, the ensuing reaction shows a fascinating mode of action − effectively reversing the growth process.[4] By exposing nanoparticles to increasing concentrations of etchant, the silver octahedral nanocrystals successively transform into truncated structures with etched edges and then back to cubic structures with slightly rough features as seen in parts A−C of Figure 1. A closer examination of these cubes reveals that their body diagonal, which corresponds to the distance between opposite faces in the original octahedral structure (part D of Figure 1), is unchanged during the reaction. Conversely, tips of the octahedra were etched to the {100}-bound faces of a cube. This clearly indicates a reversal of the reaction kinetics seen during the original overgrowth process, where {100}-bound cubes grow to become {111}-bound octahedra.[4] Briefly, the growth process proceeds more rapidly in the [100] direction, finally resulting in the {111}-bound octahedra. The observation that the $NH_4OH/H_2O_2/CrO_3$ etching mixture is selective for etching in the [100] direction encouraged further research into the optimization of this etchant system for generating plasmonic nanostructures with previously inaccessible shapes.

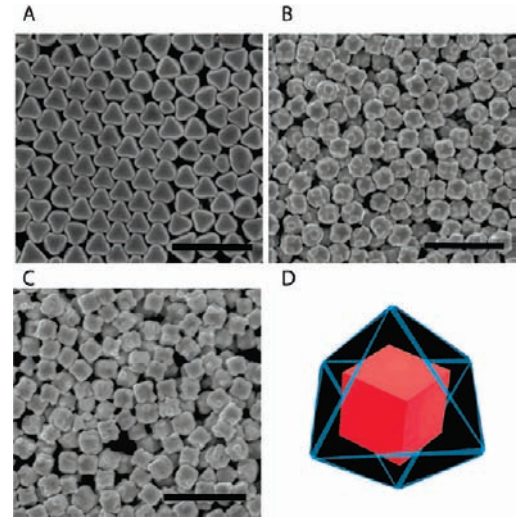

Figure 1. Etching progression of octahedra when exposed to an etchant solution containing $H_2O_2/NH_4OH/CrO_3$ in a 1:5:0.08 ratio. (A) Starting octahedra silver nanoparticles; (B) truncated structures resulting from exposure of silver octahedra to low etchant concentrations; (C) cubic particles that are formed after exposure of octahedra to higher concentrations of the etchant, all scale bars represent 1 μm; and (D) schematic representation of the resulting cube size inscribed in the starting octahedra.

Both the composition and the ratio of NH_4OH/H_2O_2 in the etchant formulation were modified to obtain a robust and safe etchant solution. Figure 2 shows the effect of removing the chromic acid from the etchant mixture; in addition to making the mixture more environmentally benign, this etchant also creates batch-scale silver nanostructures with unusual morphologies. By using a parent etchant mixture that contains 9 parts NH_4OH and 1 part H_2O_2, we were able to decrease the etching rate of exposed-edge Ag atoms, increasing the degree of anisotropic etching in the [100] direction.

Higher etching concentration increases the selective etching of {100} surfaces, resulting in concave features that eventually yield octapod structures with the same symmetry of the starting

(28) Skrabalak, S. E.; Chen, J. Y.; Sun, Y. G.; Lu, X. M.; Au, L.; Cobley, C. M.; Xia, Y. N. *Acc. Chem. Res.* **2008**, *41*, 1587–1595.
(29) Yin, Y. D.; Erdonmez, C.; Aloni, S.; Alivisatos, A. P. *J. Am. Chem. Soc.* **2006**, *128*, 12671–12673.
(30) Chen, J. Y.; McLellan, J. M.; Siekkinen, A.; Xiong, Y. J.; Li, Z. Y.; Xia, Y. N. *J. Am. Chem. Soc.* **2006**, *128*, 14776–14777.
(31) Rodriguez-Fernandez, J.; Perez-Juste, J.; Mulvaney, P.; Liz-Marzan, L. M. *J. Phys. Chem. B* **2005**, *109*, 14257–14261.
(32) Tsung, C. K.; Kou, X. S.; Shi, Q. H.; Zhang, J. P.; Yeung, M. H.; Wang, J. F.; Stucky, G. D. *J. Am. Chem. Soc.* **2006**, *128*, 5352–5353.
(33) Levinstein, H. J.; Robinson, W. H. *J. Appl. Phys.* **1962**, *33*, 3149–3152.

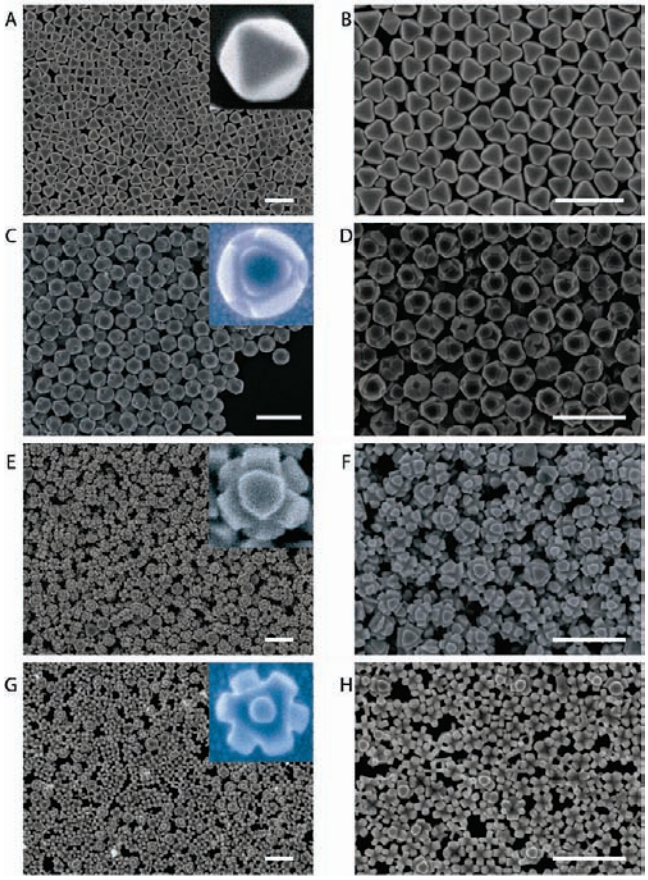

Figure 2. SEM images following the etching progress of the silver octahedral-shaped nanoparticles. (A, B) Octahedra-shaped starting material showing regular size and shape, which are essential for controlled etching reactions; (C, D) using a small amount of etchant, the edges and corners can be selectively etched leaving gaps of 5−10 nm; (E, F) when exposed to a slightly higher concentration of etching solution, eight distinct arms develop; and (G, H) finally, at relatively high concentrations of etching solution, octapod-shaped nanoparticles are isolated in high yield. All scale bars shown represent 1 μm.

octahedra (Figure 2). Multi-armed structures like our octapod have drawn attention in the past for their unique structure and plasmonic properties[3,6,34,35] but to our knowledge have not been isolated as single-crystalline uniform nanostructures in a high-yield reaction (Figure S1 of the Supporting Information for single-crystal electron diffraction).

The utility of the 9:1 NH_4OH/H_2O_2 etchant for creating new nanoparticle morphologies is schematically illustrated in part A of Figure 3, which relates the starting particle geometry and the extent of etching to the resulting complex particle shapes. These new geometries are achieved by selective etching, which occurs under kinetically controlled conditions. In contrast to the growth of these particles that occurs over the course of about an hour and relies on the stabilization of the {111} face of silver by PVP, this etching reaction runs to completion in a few seconds and allows the isolation of these complex particle geometries.

The etching rate in the [111] and [100] directions can be quantitatively evaluated by controlling the etchant concentration and measuring the average thickness of the resulting nanoparticles in both directions. Part B of Figure 3 examines the reaction kinetics of the 9:1 NH_4OH/H_2O_2 in the [111] and [100] directions. These experiments validate the selectivity of the 9:1 NH_4OH/H_2O_2 etchant formulation; the etching of {100} faces proceeds rapidly with the addition of increasing amounts of etchant solution, whereas very little etching occurs on the {111} faces. A comparison of the slope of each of best-fit lines demonstrates a greater than 20-fold preference for etching in the [100] direction. This selectivity can also be seen when the etchant is applied to cube-octahedra-shaped silver nanoparticles (parts A−C in Figure S2 of the Supporting Information). Lower etchant concentrations result in alternately exposed triangular faces {111} and recessed square faces {100}, whereas higher concentrations create a similar octapod structure. As expected by the preferential etching along the [100] direction, the etching of the cubes results in smaller cubes (parts D−F in Figure S2 of the Supporting Information).

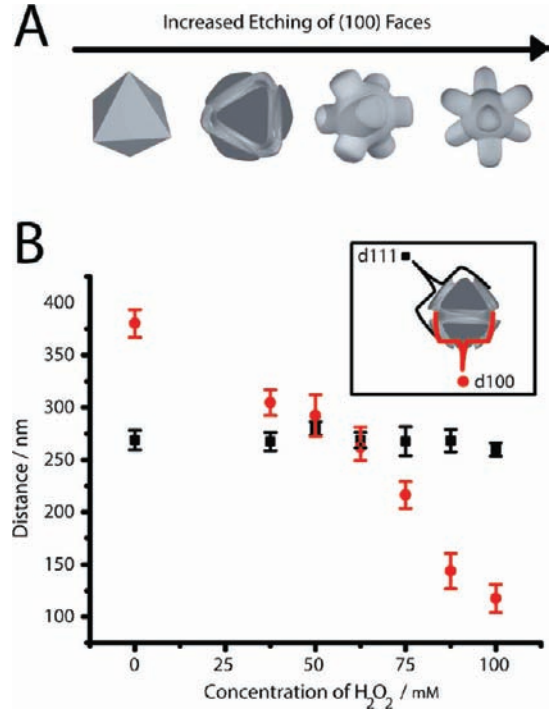

Figure 3. Mechanistic characterization of the etching procedure. (A) Schematic showing the effects of selectively etching the {100} faces of silver octahedra. (B) Plot showing the effect of etching on the thickness of {100} and {111} faces as a function of etching concentration, demonstrating the selective nature of the 9:1 NH_4OH/H_2O_2 etching solution.

From the earlier discussion of the shape-selective growth of silver nanoparticles, we have already seen increased reactivity of {100} planes during the growth phase of the reaction. It was originally postulated that the enhanced reactivity of the {100} planes was a function of both crystal habit and the presence of additional PVP as a capping agent.[4] Interestingly, the etching reactions proceed in a similar fashion without the addition of PVP but the resulting silver structures are much more susceptible to oxidation and the selectivity for the [100] etching direction is quickly diminished. These observations point to the additional importance of crystal habit on selectivity in this silver etching reaction, whereas the PVP serves to protect the silver surface from oxidation.[11]

The influence of crystal geometry has precedent in the etching literature, with similar anisotropic etching of silicon using

(34) Liu, X. H.; Huang, R.; Zhu, J. *Chem. Mater.* **2008**, *20*, 192–197.
(35) Liu, X. H.; Zhang, F.; Huang, R.; Pan, C. F.; Zhu, J. *Cryst. Growth Des.* **2008**, *8*, 1916–1923.

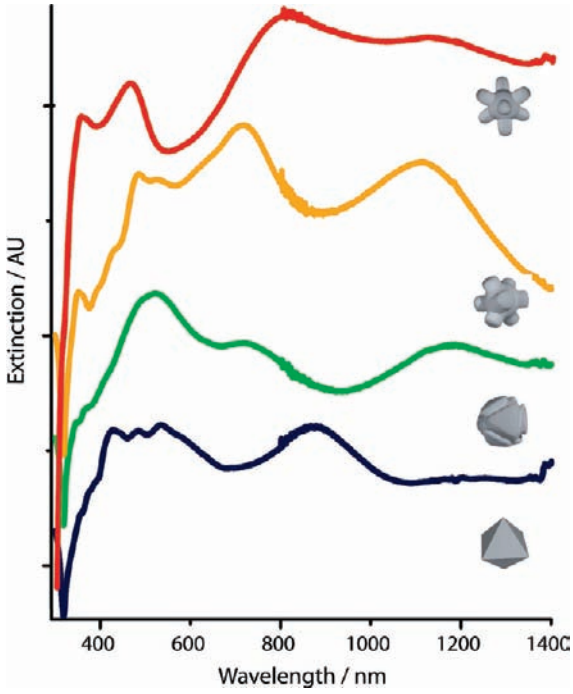

Figure 4. UV−vis−NIR characterization of the octahedral-shaped particles as a function of the etching progress when starting from octahedral nanoparticles. Interestingly, as the etching progresses the octapod structures have LSPs with greater intensity in the red and near-infrared regions.

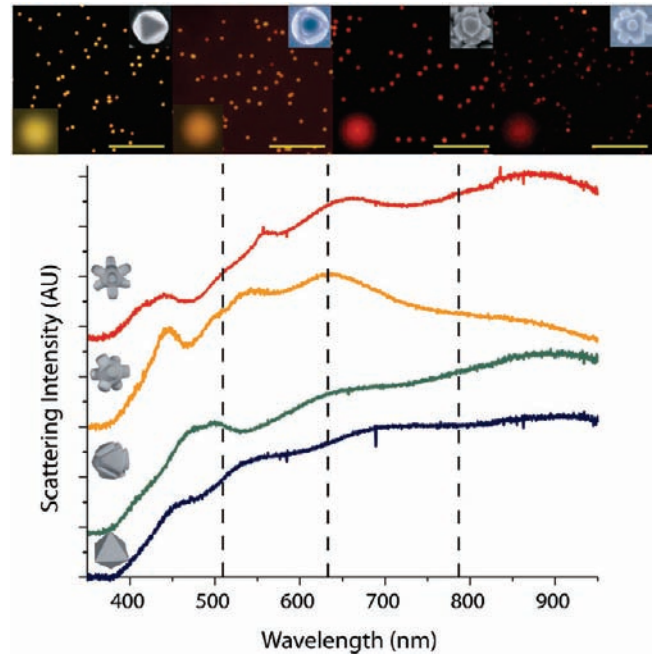

Figure 5. Single-particle scattering spectra for each of the four stages of etching starting from octahedral-shaped particles. The overlaid lines in the spectra demark the excitation wavelengths used for the single-particle SERS experiments. Images on the top of the spectra show particle shape and real-color darkfield images. Scale bars represent 20 μm.

alkaline solutions[36] without additional capping agents. Seidel and co-workers evaluated three competing explanations for the anisotropic etching of silicon in alkaline solutions: (1) the bond density on various crystallographic faces, that is surface energy; (2) selective protection of {111} faces by oxide; (3) the activation energy for the different backbonded geometries of each face produces a kinetic barrier to etching {111} planes. They found that the influence of the activation energy correlates best with the 100:1 rate enhancement of etching in the [100] direction. This explanation is compelling in the silver system, given the similarity of the crystal geometries, the kinetically controlled etching solutions, and a similar difference in etching rates along the [100] and [111] directions.

To better understand the modification of plasmonic features, which result from the changing particle shape, we examined the progression of etching in the octahedra nanoparticle system. The dramatic changes caused by etching can be seen during the reaction−upon the addition of particles to the etching solution the color changes from tan, to yellow, then orange, followed by purple and finally pinkish red for octapod solutions. These changes were followed by UV−vis−NIR spectroscopy and are shown in Figure 4. As the amount of etchant increases, intense localized surface plasmon bands appear in the red and infrared regions of the extinction spectrum. The extinction onset of the starting octahedra (blue trace in Figure 4) shows significant scattering from 400−600 nm. The concave features of the mildly etched particles (green trace in Figure 4) introduce new plasmonic bands with a strong intensity between 550−800 nm in the extinction spectrum. In addition to changing the LSPs, these mildly etched structures provide new gaps, corners, and edges where local hotspots could lead to enhanced electric fields for spSERS. The final octapod structure (red trace in Figure 4) shows the most dramatic change in the extinction profile. The major features are found in the red with the dominant feature appearing at 750 nm and extending well into the near IR. In addition to the strong LSPs in the red, there are also new LSPs at 400 and 500 nm (more extinction spectra following the etching process are shown in Figure S3 of the Supporting Information).

Similar multi-arm gold structures reported by Nehl et al. have also demonstrated novel plasmonic characteristics with strong responses to changes in dielectric environment.[3] The LSPs for many previously reported silver nanostructures are typically located in the visible region. Previous reports of silver plasmon bands shifted to the red and near-infrared were often achieved through interparticle coupling[17] or with structures that are very large (>1 μm).[37] Our 250 nm octapod structures show strong scattering in the NIR, resulting from the intraparticle gaps formed during the etching process, making them attractive for single-particle applications in biology. More importantly, the vis−NIR tunability of the plasmonic response is accomplished by a simple chemical etching process.

Single-particle scattering spectra were obtained to correlate with the UV−vis extinction spectra (Figure 5). Particles were prepared for imaging by drop-casting onto a glass coverslip.[4] The single-particle scattering spectra correlate well with the extinction spectra, indicating that the plasmon bands seen in the UV−vis−NIR are intrinsic features of these etched particles with complex geometries. Darkfield microscopy also reveals a perceptible change in the color of the scattered light as seen in the real-color digital images of the single particles, shown to the right of each darkfield spectra in the top of Figure 5. The color of the scattered light changes from yellow-green for the octahedra, to orange for the mildly etched structures, and finally becoming red for the octapod structures.

(36) Seidel, H.; Csepregi, L.; Heuberger, A.; Baumgartel, H. *J. Electrochem. Soc.* **1990**, *137*, 3612–3626.

(37) Xiong, Y.; Washio, I.; Chen, J.; Sadilek, M.; Xia, Y. *Angew. Chem. Int. Ed.* **2007**, *46*, 4917–4921.

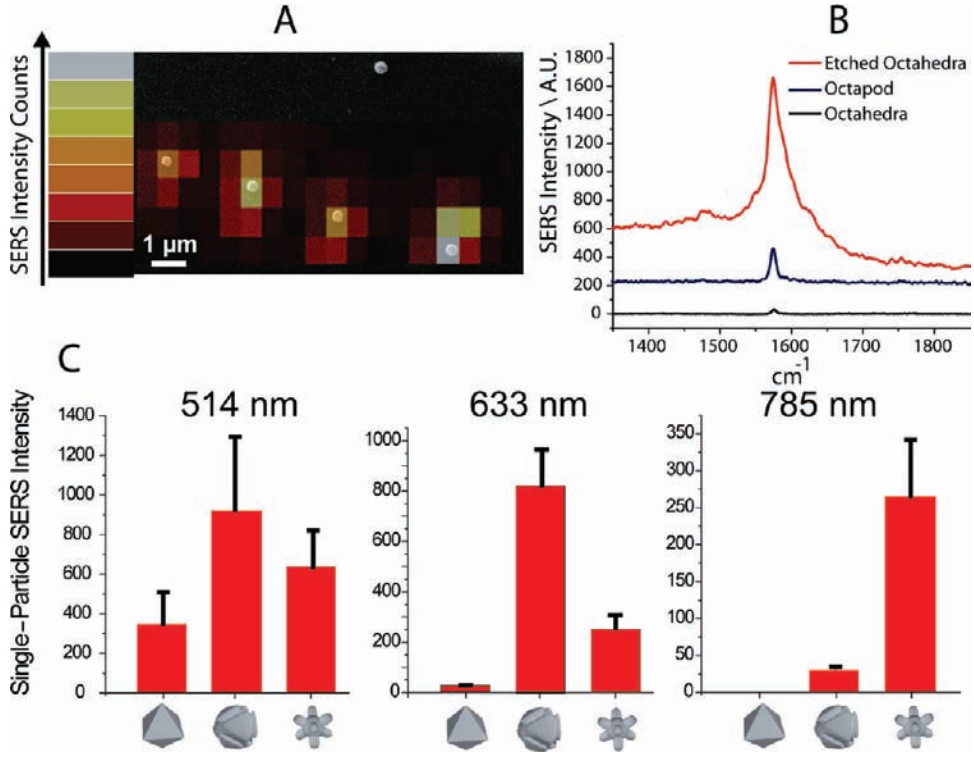

Figure 6. Single-particle Raman scattering of benzenethiol at 1584 cm^{-1}. (A) SEM image of isolated, etched particles overlaid with the SERS intensity map, color are assigned by the relative intensity of the spectrum at 1584 cm^{-1}; (B) representative SERS spectra for each shape obtained during 1 s integration with 633 nm excitation; and (C) average single-particle intensity shown for each particle shape as a function of excitation wavelength. Error bars reflect one standard deviation.

The unique structural features and broad resonance response of the etched nanoparticles allow us to carry out spSERS at three different wavelengths (514, 633, and 785 nm) using benzenethiol as a nonresonant analyte. The exchange of PVP on the surface of the silver particles was achieved by soaking the particles in a 20 mM ethanolic solution of benzenethiol for 12 h.[11] Single particle Raman spectra were obtained using a Renishaw inVia confocal Raman microscope system with a mapping stage allowing 500 nm resolution. Dilute solutions of each of the particle shapes were prepared and drop-cast onto patterned substrates for Raman and SEM mapping. Seen in part A of Figure 6 are overlays of the Raman map on top of the corresponding SEM image ensuring only single particles were sampled. Each pixel corresponds to a 500 × 500 nm area and the colors represent changes in the intensity of the benzenethiol peak at 1584 cm^{-1}. The interparticle spacing is sufficiently large to ensure no particle coupling is taking place. Part B of Figure 6 shows typical spectra obtained during the mapping experiment, demonstrating a very good signal-to-noise ratio even with a 1 s integration time. Using this technique on three of the distinct particle shapes allowed us to study the effect of excitation wavelength on the spSERS response.

Previous reports have documented the SERS activity that can be optimized when the excitation source is matched to the plasmonic resonance of the metal nanostructures.[38] A similar wavelength-dependent SERS activity is also seen for these etched particles in part C of Figure 6, where the signal response for each of the particles is comparable with 514 nm excitation. As the excitation wavelength moves to the red, first the mildly etched particles (633 nm) and then octapod particles (785 nm) selectively produce spSERS signals with high intensities. Enhancement factors have been calculated using the expression $EF = (I_{surface})/(I_{solution}) \times N_{solution}/N_{surface}$ where $N_{solution}$ and $N_{surface}$ are the number of molecules probed in a standard solution and on the substrate respectively, and $I_{solution}$ and $I_{surface}$ correspond to the normal and SERS signal intensities, respectively.[39] Enhancement factors for each of these shapes at their optimal excitation wavelength range from 3×10^4 for a single octahedra to 5×10^5 for both the mildly etched octahedra and the octapod structures. Although these enhancement factors seem modest, they represent a minimum value averaged over the surface of these nanoparticles. The actual enhancement of the SERS signal is taking place at regions of these particles with high local electric fields including corners and for the etched structures intraparticle gaps but the error associated with an estimation of hotspot area is unacceptably high. Regardless of EF, these particles demonstrate both strong signal response and wavelength-dependent behavior, making them attractive for multiwavelength imaging and tagging applications.

To understand this change in spSERS intensity, it is important to consider how the wavelength-dependent intensity correlates with the dimensions of the gaps, tips, and edges where hotspots are located. For example, the UV−vis−NIR and single-particle scattering spectra indicate that new local surface plasmons appear in the red and infrared as the octahedra particles are increasingly etched. This result corroborates well with the sensing experiment, where the spSERS signal at 785 nm gets better as the octahedra are etched progressively into octopods. Because the starting octahedra are large, both the extinction and the scattering spectra of the octahedra demonstrate significant

(38) McFarland, A. D.; Young, M. A.; Dieringer, J. A.; Van Duyne, R. P. *J. Phys. Chem. B* **2005**, *109*, 11279–11285.

(39) Nikoobakht, B.; Wang, J. P.; El-Sayed, M. A. *Chem. Phys. Lett.* **2002**, *366*, 17–23.

interaction with light at 785 nm but the spSERS experiment with 785 nm excitation fails to yield any appreciable signal. This observation can only be explained if the unique nature of the intraparticle gaps is taken into account, indicating that the new peaks in the red region of the spectra for the etched structures correspond to more localized LSPs than those in the starting octahedra. The unique nature of the intraparticle gaps is further supported by the observation that the etched particles outperform the parent octahedra structure by 5−50 fold at all wavelengths. Previous results have shown the importance of nanoscale gaps for SERS enhancement,[5,22] and we believe that the nanoscale intraparticle gaps in these structures are essential to the performance of our particles.

Conclusions

In summary, we have demonstrated a novel anisotropic etching methodology for the synthesis of complex nanoparticle shapes. By optimizing the etching solution for maximum selectivity and environmental compatibility, we have devised a robust etching formulation for silver nanoparticles. Controlling the kinetics and selectivity of etchant solutions is a simple new way to achieve highly anisotropic nanoparticle shapes. The interesting optical properties of these nanostructures have been characterized and they have plasmon bands spanning the visible spectrum and into the infrared. Tuning single-particle LSP peaks across the visible and into near IR portion of the electromagnetic spectrum makes these silver nanoparticles attractive for many plasmonic-based applications. In particular, these etched particles can function as highly sensitive spSERS substrates. In the future, these particles will be incorporated into multiplexed sensors for the simultaneous detection of multiple analytes.

Acknowledgment. The authors acknowledge the DARPA SERS program for funding. Martin Mulvihill also acknowledges financial support from the Superfund Office of Basic Research and Xing Yi Ling thanks the Rubicon grant from Netherlands Organization for Scientific Research (NWO) for the financial support. The authors would like to thanks Dr. Dan Gargas for helpful discussions and assistance editing the manuscript. Additionally the authors thank Jean Benjauthrit for her assistance during the early stages of this project.

Note Added after ASAP Publication. In the version of this paper published ASAP on Dec 10, 2009, the volume of silver nitrate solution injected per minute in the nanoparticle synthesis was given as 500 mL. This was changed to 500 μL in the corrected version published ASAP on Dec 15, 2009.

Supporting Information Available: Additional figures and a table of associated redox potentials This material is available free of charge via the Internet at http://pubs.acs.org.

JA906954F